

A study on convection in molten zone of aluminum alloy during Fe/Al resistance spot welding

Muneyoshi Iyota^{a,*}, Tomoki Matsuda^b, Tomokazu Sano^b, Masaya Shigeta^c, Takahisa Shobu^d, Hirokatsu Yumoto^{e,f}, Takahisa Koyama^{e,f}, Hiroshi Yamazaki^{e,f}, Yasunori Senba^{e,f}, Haruhiko Ohashi^{e,f}, Shunji Goto^{e,f}, Ichiro Inoue^f, Yujiro Hayashi^f, Kenji Tamasaku^f, Taito Osaka^f, Jumpei Yamada^f, Makina Yabashi^f

^a Department of Mechanical Engineering, Faculty of Engineering, Osaka Institute of Technology, 5-16-1 Omiya Asahi-ku, Osaka 535-8585, Japan

^b Division of Materials and Manufacturing Science, Graduate School of Engineering, Osaka University, 2-1 Yamadaoka, Suita, Osaka 565-0871, Japan

^c Division of Mechanical Engineering, Graduate School of Engineering, Tohoku University, 6-6-1 Aoba, Aramaki, Aoba-ku, Sendai 980-8579, Japan

^d Materials Sciences Research Center, Japan Atomic Energy Agency, 2-4 Shirakata, Tokai-mura, Ibaraki 319-1195, Japan

^e Japan Synchrotron Radiation Research Institute, 1-1-1 Kouto, Sayo-cho, Sayo-gun, Hyogo 679-5198, Japan

^f RIKEN SPring-8 Center, 1-1-1 Kouto, Sayo-cho, Sayo-gun, Hyogo 679-5148, Japan

ARTICLE INFO

Keywords:

Resistance spot welding
Dissimilar materials joining
Aluminum alloy
Convection
Direct observation
Synchrotron radiation X-ray

ABSTRACT

Aluminum alloys are increasingly being applied to automobile bodies to reduce the weight of automobiles. In joining steel materials and aluminum alloys using resistance spot welding (RSW), it is important to control the state of intermetallic compounds due to the temperature at the joining interface. In other words, in RSW of Fe/Al dissimilar materials, it is necessary to clarify the heating and cooling phenomena of the interface temperature during joining. Although the convection behavior of the molten aluminum alloy is thought to influence the temperature distribution at the joining interface, there are no studies that have directly observed this phenomenon. In this study, convection in molten zone of aluminum alloy during RSW of steel and aluminum alloy is discussed. Direct observations were attempted in order to clarify the convection behavior of the molten aluminum alloy in RSW of steel and aluminum alloy. The main feature of this experiment is that a real-scale test piece and an RSW apparatus used in actual production were used to observe convection during actual production. The observation experiments were conducted using synchrotron radiation X-ray at SPring-8. During welding, the specimens were irradiated with synchrotron radiation X-ray, and convection was observed from the behavior of tracer particles placed on the specimens. As a result, three types of convection were observed: radial outward convection from the center of the molten zone at the joining interface, convection from the edge of the molten zone toward its center, and weak circulating convection at the edge of the molten zone. And, small convection velocities were generated at the edge of the molten zone. Furthermore, the convection velocity inside the molten zone was calculated to be approximately 1.75 m/s. In addition, it was shown that there is a correlation between convection behavior and the shape of the molten zone.

1. Introduction

In recent years, the automotive industry has been promoting fuel-efficient automobiles from the viewpoint of vehicle emissions regulations. One of these measures is to reduce the weight of automobile bodies. In addition to using ultra-high-strength steel sheets to reduce plate thickness, light metals, such as aluminum alloys and magnesium alloys, are used in areas where strength is unnecessary. In particular, the

application of aluminum alloys has attracted the most attention, and research is being conducted on hybrid structures that combine conventional steel materials with aluminum alloys. In order to achieve this hybrid structure, it is necessary to join dissimilar materials, such as steel and aluminum alloy. Various methods, such as resistance spot welding (RSW) [1–14], friction stir spot welding (FSSW) [15], and laser welding [16], have been investigated for this purpose. In particular, much research has been done on RSW, because it can be carried out using

* Corresponding author.

E-mail address: muneyoshi.iyota@oit.ac.jp (M. Iyota).

<https://doi.org/10.1016/j.jmapro.2023.03.032>

Received 1 November 2022; Received in revised form 5 March 2023; Accepted 12 March 2023

Available online 5 April 2023

1526-6125/© 2023 The Author(s). Published by Elsevier Ltd on behalf of The Society of Manufacturing Engineers. This is an open access article under the CC BY-NC-ND license (<http://creativecommons.org/licenses/by-nc-nd/4.0/>).



Fig. 1. Photograph of tilted welding equipment.

existing production equipment.

When dissimilar materials such as steel and aluminum alloy are joined using RSW, an intermetallic compound is formed at the joining interface. It is known that this intermetallic compound is formed by the interdiffusion of Fe and Al atoms, depending on the temperature field at the joining interface. Therefore, much research has been conducted on

RSW of dissimilar materials such as steel and aluminum alloy. In particular, recently, in addition to research on the understanding of IMC properties [1–6], research focusing on electrode geometry [7–11], research using intermediate layers [12,13], and research using external magnetic fields [14] has been conducted to control IMC properties. All of these studies have investigated how to control intermetallic properties thermally or microstructurally, i.e., the physical phenomena at the joining interface. On the other hand, temperature field around joining interface is considered to be determined by the balance between heat generation due to the specific resistance of the steel and aluminum alloy and heat removal due to heat conduction. In addition, since the joint interface is always in contact with the aluminum alloy melt during welding, the dynamic behavior of the molten aluminum alloy, in other words, convection, is expected to affect the temperature field.

Convection of molten metal has been studied extensively in arc welding and laser welding [17–26]. In the case of arc welding, studies have been conducted using simulations and direct observations, and, similarly, in the case of laser welding, direct observations have been conducted. There have also been several numerical simulation studies on the convection behavior of molten metal in RSW [27]. However, all of these studies were conducted for similar materials RSW, and there are few examples of dissimilar materials, such as steel and aluminum alloy [28]. In addition, the accuracy of the numerical simulations cannot be verified due to the lack of experimental data for convection in molten

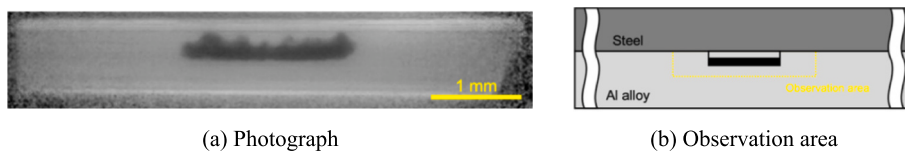


Fig. 2. Initial position of tracer particles.

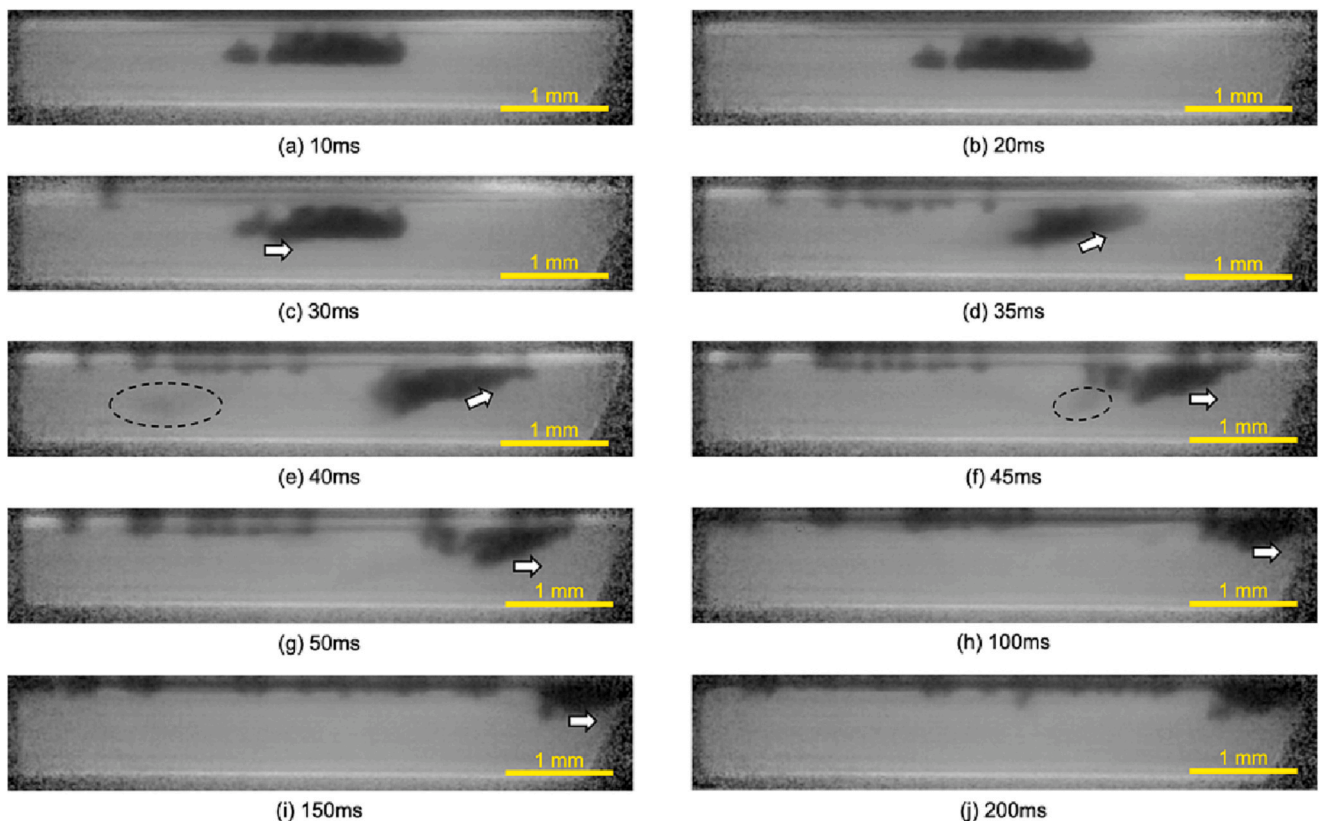


Fig. 3. Behavior of tracer particles during current application.

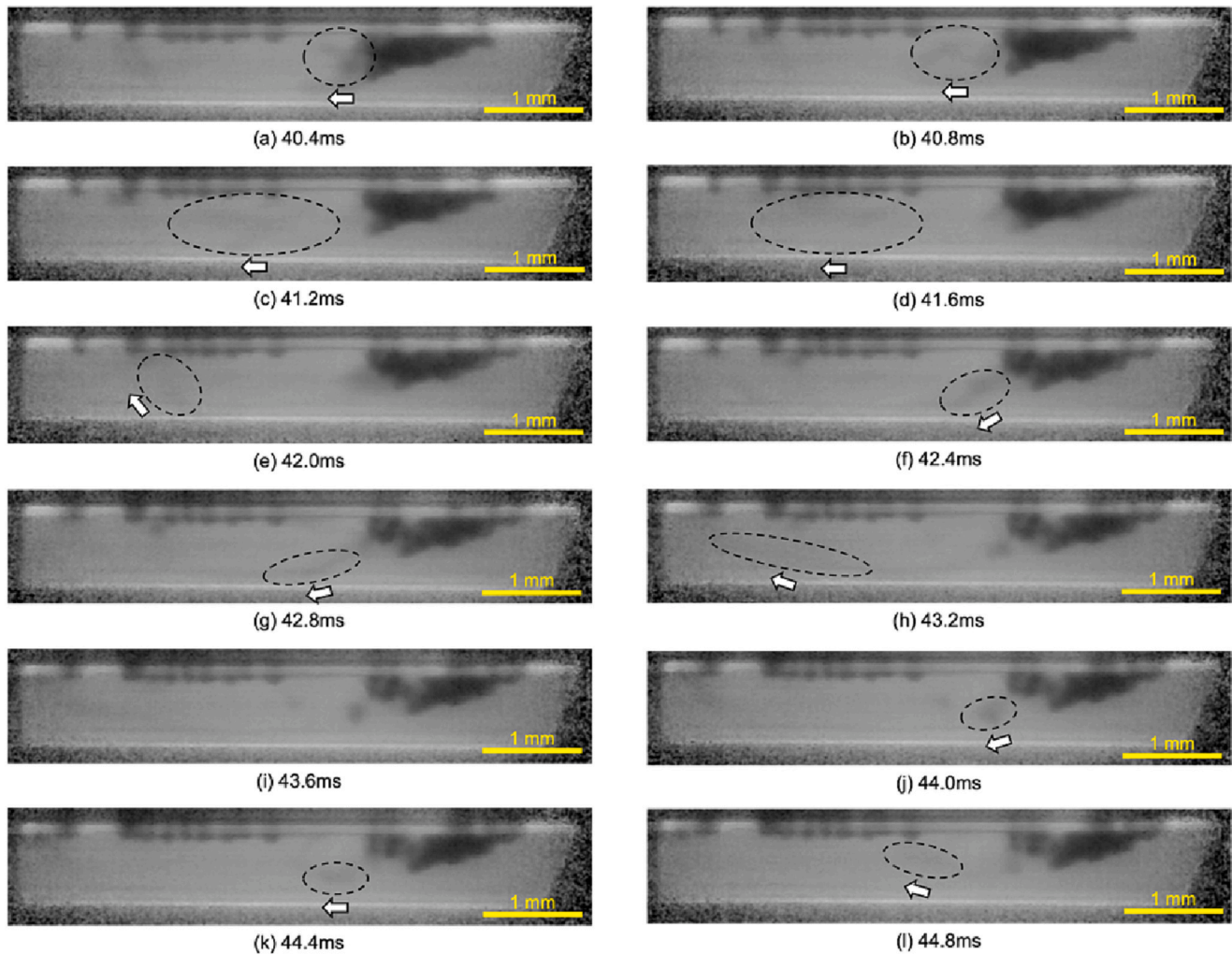


Fig. 4. Convective flow toward molten zone.

aluminum alloy, and the physical phenomena have not yet been clarified.

In this study, direct observations were attempted in order to clarify the convection behavior of the molten aluminum alloy in RSW of steel and aluminum alloy. The main feature of this experiment is that a real-scale test piece and an RSW apparatus used in actual production were used to observe convection during actual production. Furthermore, the use of synchrotron radiation X-ray at SPring-8 enabled direct observation of convection behavior. By observing the behavior of tracer particles set in aluminum alloy, the direction and velocity of convection during RSW were measured, and the relationship between the shape of the molten zone and convection behavior is discussed.

2. Materials and experimental procedure

2.1. Materials

A 1.2 mm-thick hot-dip galvanized alloyed steel sheet (GA590) and a 1.6 mm-thick aluminum alloy sheet (A6061) were used as test materials. The chemical compositions of each material are shown in Table 1. The dimensions of the specimen was 50 mm × 50 mm.

2.2. Welding procedure

A C-type gun RSW system with a DC inverter power supply was used for welding. An R-type electrode tip with a tip curvature of 100 mm

made of alumina dispersion strengthened copper was used. The welding conditions during convection observations were a current of 14 kA, a current application time of 200 ms, and an electrode force of 5.0 kN. The current was changed to 11 kA when calculating the convection velocity. In both welding conditions, GA590 was set on the positive electrode side and welding was conducted.

Tungsten (W) particles were used as tracer particles, with sizes of 150 μm and 25 μm for the observation of convection and 53 μm for the calculation of convection velocity, respectively. The tracer particles were filled into the holes on the aluminum alloy side in appropriate quantities. The holes were 2 mm in diameter and 0.4 mm in depth for the convection observation and 1 mm in diameter and 0.4 mm in depth for the convection velocity observation.

2.3. In-situ observation

The experiment was conducted at the RIKEN Contract Beamline BL05XU at SPring-8. In this experiment, 100 keV light with an energy bandwidth of approximately 0.93 % was used, which was formed by shaping 100 keV light, the primary light of the 5.26 keV fundamental wave from the undulator, using a multilayer mirror. This X-ray beam was further shaped with a slit, and a 0.7 mm (length) × 4.0 mm (width) X-ray beam irradiated a test specimen placed in the center of a RSW apparatus installed in an optical hutch. The transmitted X-ray was observed with a CsI scintillator located 1.5 m downstream, and the converted visible light was measured with a high-speed camera

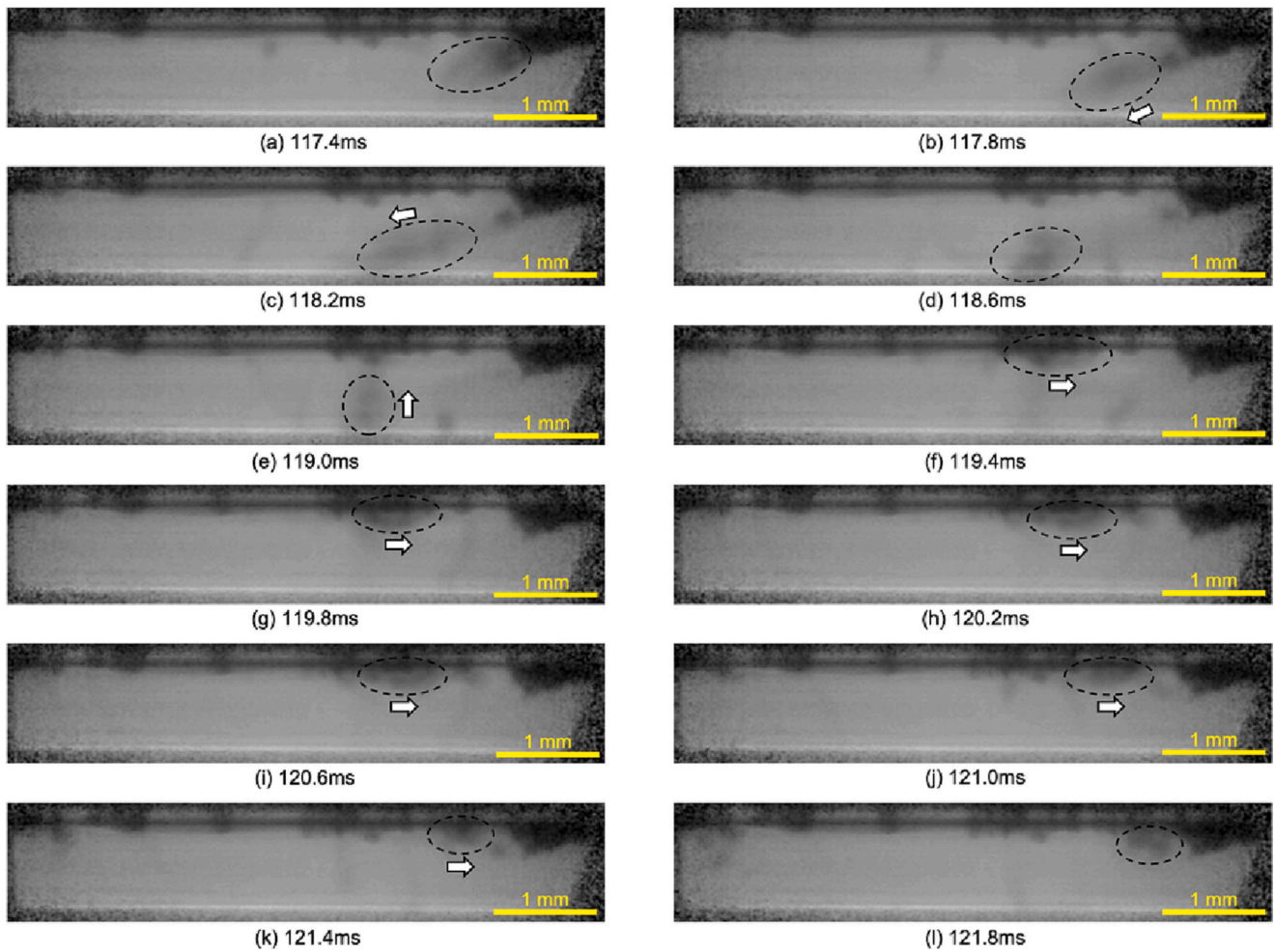


Fig. 5. Convection current circulating at edge of molten zone.

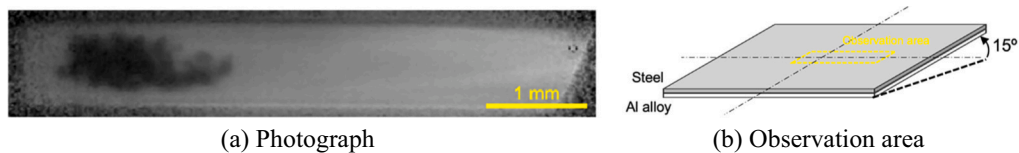


Fig. 6. Initial position of tracer particles when welding equipment is tilted by 15°.

manufactured by nac Image Technology Inc. The pixel resolution was approximately 15 μm , and time-resolved measurements were made at 2500 Hz and 5000 Hz. Using this system, convection currents inside the molten aluminum alloy during welding were observed based on the movement of tracer particles.

In addition to the normal welding posture, in which the welding apparatus was installed perpendicular to the ground to observe convection in the cross-sectional direction of the molten zone, a tilted posture was used to investigate three-dimensional convection phenomenon in the molten zone. During tilted welding, as shown in Fig. 1, the welding apparatus was tilted 15° to the upstream of the beam, and X-ray irradiation was from the steel side toward the center of the weld.

2.4. Cross-sectional and microstructure observation

Cross-sectional and microstructural observations were conducted to observe the shape and microstructure of the molten zone of joints. For cross-sectional observation, 3 % nital was used as the etching solution,

and the shape of the molten zone was observed using a microscope. For microstructural observation, 5 % hydrofluoric acid was used as the etching solution, and SEM was used to observe the microstructure.

3. Results

3.1. Overview of convection

Fig. 2 shows the initial state of the 150 μm tracer particles. A small amount of particles are concentrated in a hole with a diameter of 2 mm and a depth of 0.4 mm, indicating the presence of tracer particles inside the aluminum alloy plate.

Next, Fig. 3 shows the movement of tracer particles during current application. As shown in Fig. 3(a) and (b), there is almost no movement of the particles until 20 ms after the start of current application. This is probably due to the fact that the molten zone is small or hardly formed, and convection currents are not sufficient to move the tracer particles. On the other hand, at 30 ms, the particles begin to move in the direction

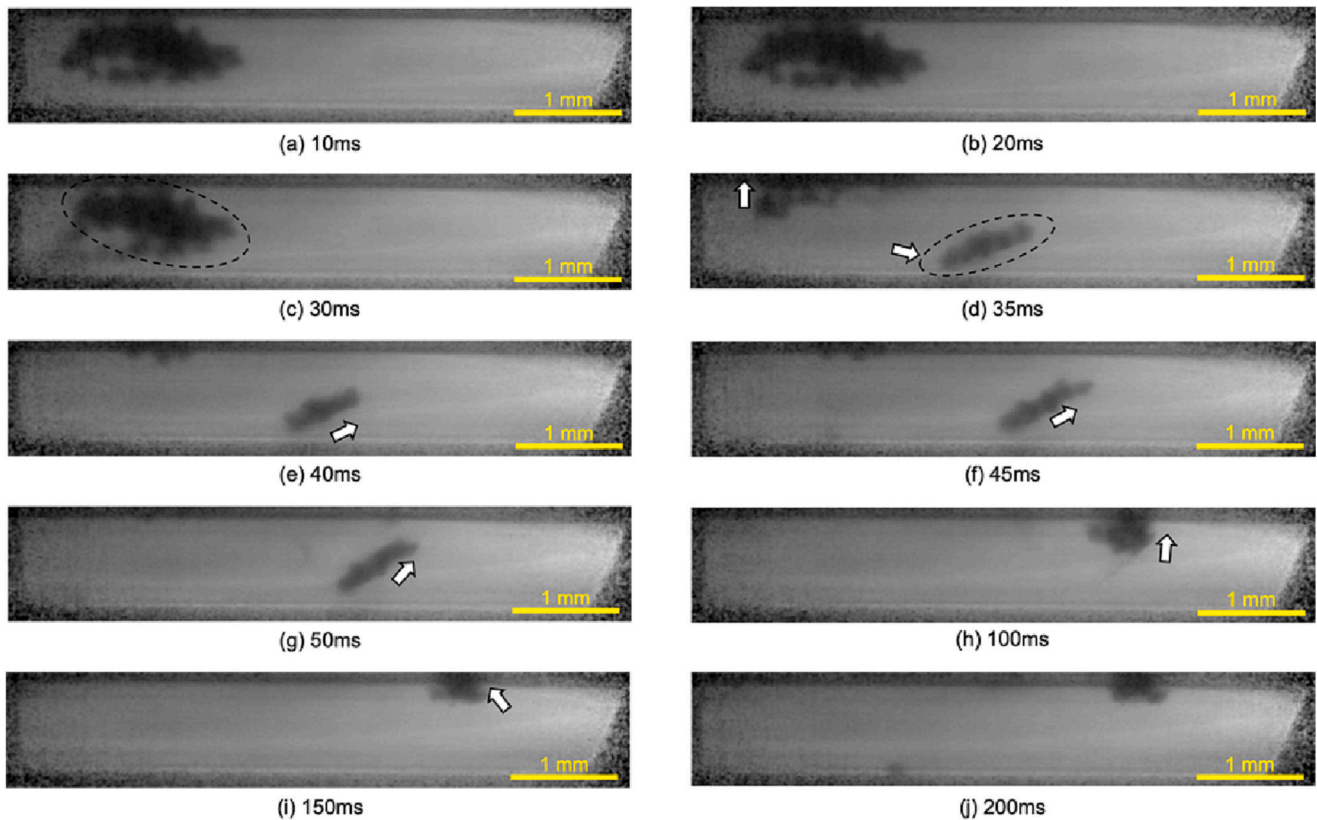


Fig. 7. Behavior of tracer particles during current application when welding apparatus is tilted by 15°.

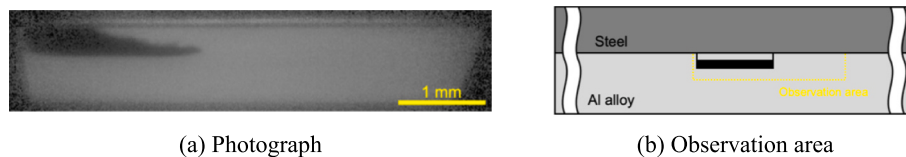


Fig. 8. Initial position of 25 μm tracer particles.

of the arrow in the figure, and at 35 ms, the particles move significantly outward in the radial direction from the center of the molten zone. Furthermore, the particles move radially outward along the joining interface as the current application time increases. On the other hand, as shown in Fig. 3(e) and the dashed lines in Fig. 3(f), a flow of particles returning from the large clumps to the center of the molten zone can be observed, but the motion of particles cannot be captured with a time resolution of 5 ms. In order to confirm the details of the motion of these particles, detailed images were obtained for the motion of the particles from 40 to 45 ms, observed every 0.4 ms, and the results are shown in Fig. 4. It can be seen that some particles peeled off from the particles that were accumulated at the edge, and moved in an arc toward the center of the molten zone. The particles were constantly moving, and the large movement of particles within 1 ms suggests that the convection velocity is extremely high. Next, Fig. 5 shows the observation results during the middle stage of current application. The particles detached from the accumulated particles at the edge are moving toward the center of the molten zone while drawing an arc. This is similar to the movement of particles shown in Fig. 4. However, the particles stop moving toward the center in the middle of the arc, and then move toward the interface. The particles then move outward in the radial direction and merge with the accumulated particles. While there is convection from the edge toward the center of the molten zone, as shown in Fig. 4, there is a small amount of convective circulation at the edge of the melt, as shown in Fig. 5.

Thus, the observations in Fig. 3, Fig. 4 and Fig. 5 indicate that convection flows radially outward from the center of the molten zone toward the outside of the molten zone at the interface, from the edge toward the center of the molten zone, and then at the edge of the molten zone.

In order to obtain depth information, i.e., the circumferential flow during convection, the welding apparatus was tilted, and the behavior of the particles was observed from the top of the specimen. Fig. 6 and Fig. 7 show the initial filling positions of the particles and the observation results of the tracer particles during the current application process, respectively. The particles placed at the center of the weld (the leftmost particle in the image) began to move 30 ms after current application. Subsequently, most of the particles moved to the upper side of the image, whereas some moved to the edge of the molten zone at the lower right of the image, as shown by the dashed line. This shows that the particles that accumulate circumferentially at the edge of the molten zone are slowly moving along the edge of the molten zone as the current is applied. This movement is extremely slow compared to the movement of the particles shown in Fig. 4, suggesting that the convection velocity is extremely small at the edge of the molten zone.

3.2. Convection at edge of molten zone

Using 150 μm tracer particles, characteristic convection was found not only inside the molten zone but also at its edge. To observe the

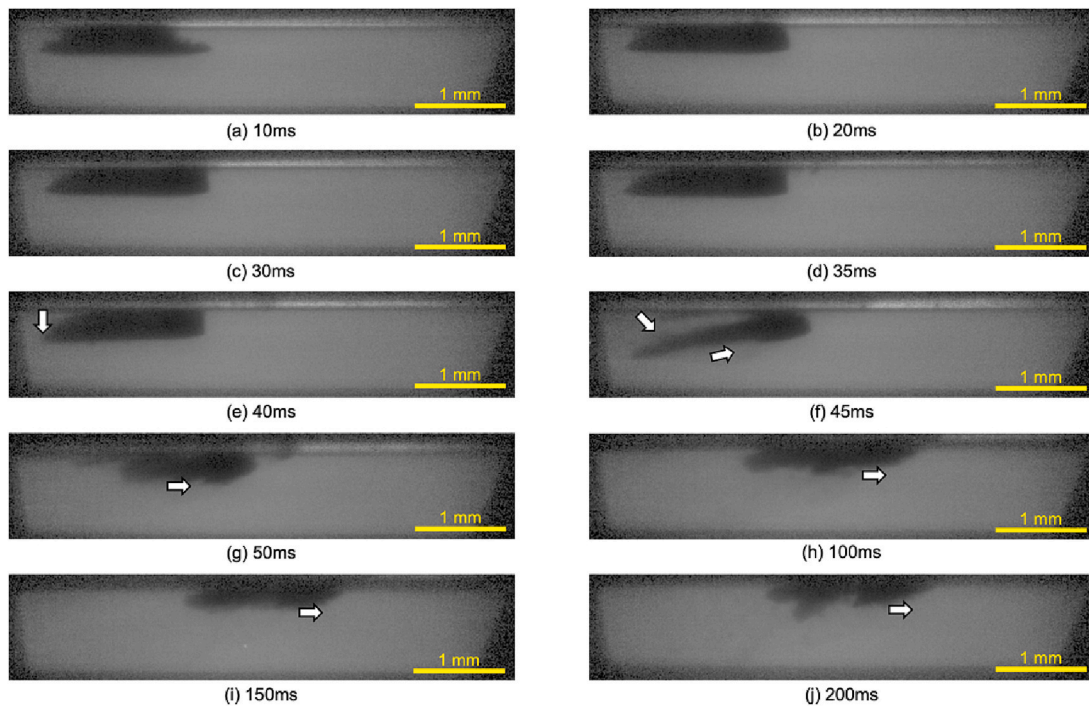


Fig. 9. Tracer particle convection at edge of molten zone.

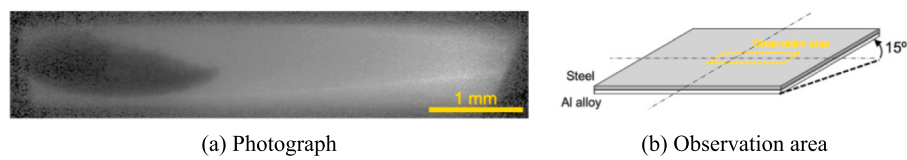


Fig. 10. Initial position of 25 μm tracer particles when welding equipment is tilted by 15°.

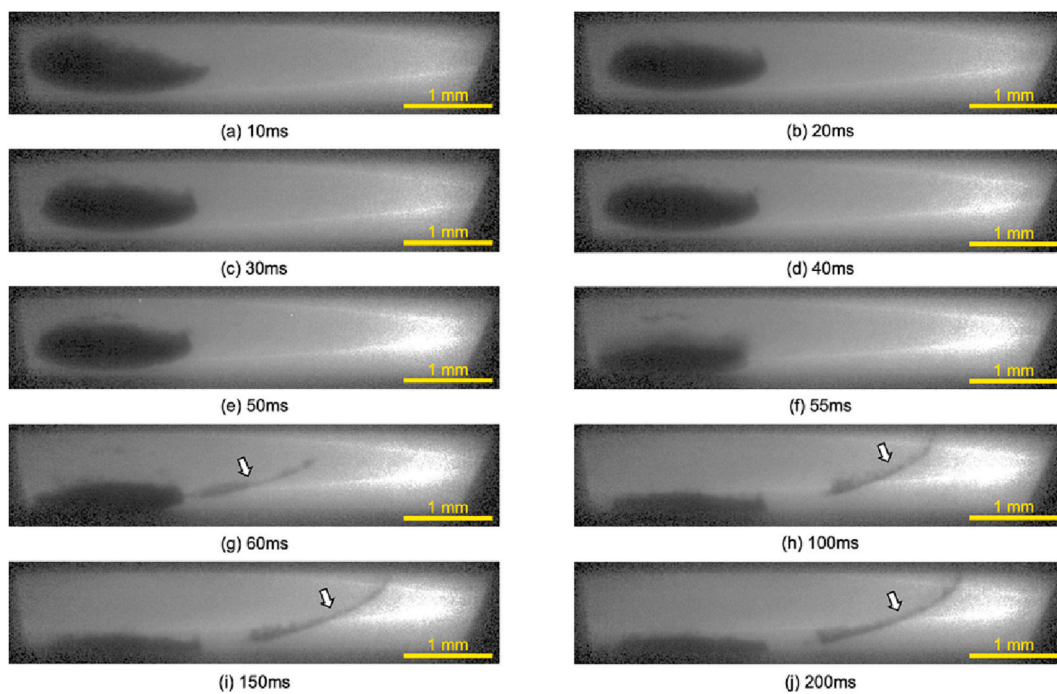


Fig. 11. Behavior of 25 μm tracer particles during current application when welding apparatus is tilted by 15°.

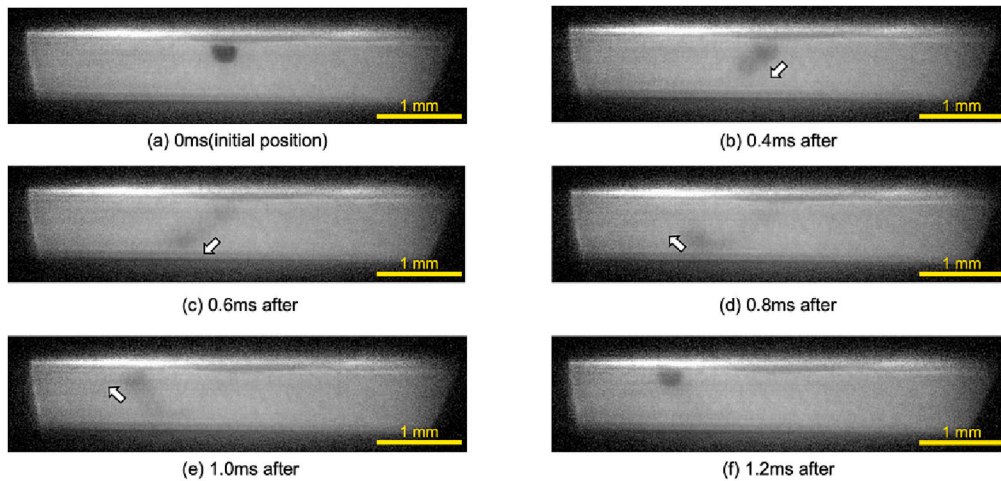


Fig. 12. Motion of tracer particles when calculating convection velocity.

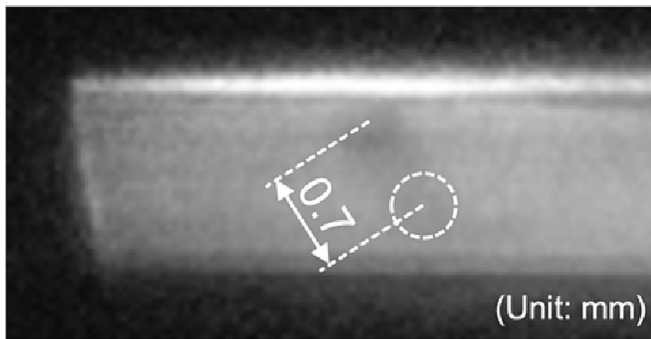


Fig. 13. Particle movement distance during period of 0.2 ms.

convection at the edge of the molten zone in more detail, tracer particles with a size of $25\ \mu\text{m}$ were used. Fig. 8 and Fig. 9 show the initial filling positions for the particles and the observation results during current application, respectively. The observation position is the edge of the molten zone, and the welding center is at the right edge of the image. As indicated by the white arrows, the tracer particles begin to move significantly 40 ms after the start of current application, and the particles move to the edge of the molten zone and then outward in the radial direction as the molten zone expands. And the particles that move to the edge form clumps. These results are similar to those using $150\ \mu\text{m}$ tracer particles. Therefore, it can be inferred that convective flow at the edge of the molten zone is small enough to prevent the particles from moving significantly.

Next, the behavior of the particles at the edge of the molten zone was observed from the top of the specimen by tilting the welding apparatus. Fig. 10 and Fig. 11 show the initial filling positions for the particles and the observation results for tracer particles during current application, respectively. After particles moved to the bottom of the image at 50 ms from the start of current application, the white arrows in the figure show that the particles that initially moved to the edge of the molten zone, later spread along its edge from 60 ms onward. Furthermore, these particles do not move significantly during subsequent current application. This is similar to the case for $150\ \mu\text{m}$ tracer particles, suggesting once again that there may be a region at the edge of the molten zone where convection is extremely small.

3.3. Convection speed

As described above, a rough understanding of the convection that

occurs in the molten zone was obtained in this experiment. However, the convection velocity was not clarified. Fig. 12 shows the results of observations using only a few $53\ \mu\text{m}$ tracer particles. The particles are moving near the edge while forming a V-shape. The speed of movement was calculated from the relationship between the amount of movement of the particles and the elapsed time. As shown in Fig. 13, the particles move a distance of 0.7 mm in 0.2 ms, giving a movement speed of approximately 1.75 m/s. This speed is close to the value obtained for laser welding [20], indicating that the same level of convection occurs in RSW.

4. Discussion

4.1. Relationship between the shape and microstructure of the molten zone and convection

Fig. 14 shows cross-sectional images taken at different current application times. For the initial time of 33 ms, the molten zone is shallow and grows slightly in the radial direction, but is still extremely small. At 50 ms, it grows in the radial direction and becomes larger in the thickness direction. Thereafter, it continues to grow in both the radial and thickness directions as the current continues to flow. After 67 ms, when the molten zone has grown to a certain extent, a shallow melted region is observed at the edge of the molten zone, and this region grows rapidly inward.

Next, the effect of convection on the macroscopic expansion behavior of the molten zone is discussed. As shown in Fig. 14(a), when a current is applied and a thin molten zone is formed at the interface, as shown in Fig. 3(d), convection occurs in the radial direction in the molten zone. Subsequently, as shown in Fig. 14(b), the molten zone grows in the direction of the plate thickness, as shown in Fig. 4, and convective flow occurs in an arc from the edge of the molten zone toward the center of the weld while expanding in the direction of the plate thickness. When the molten zone grows rapidly in the thickness direction, as shown in Fig. 14(e) and (f), a circulating convective flow is generated at the edge of the molten zone, as shown in Fig. 5. These results indicate that convection is caused by macroscopic expansion of the molten zone. However, the direct effects of these phenomena are unknown at this stage and will be discussed in a follow-up report.

Moreover, the microstructure of the molten zone is discussed. Fig. 15 shows an SEM image of the molten zone of aluminum alloy. Fig. 15(a) shows the locations where microstructural observations were conducted, and Fig. 15(b) to (e) show the microstructures at locations (b) to (e) in the Fig. 15(a), respectively. The direction of convection in the microstructure at each location is also shown at the SEM images, as

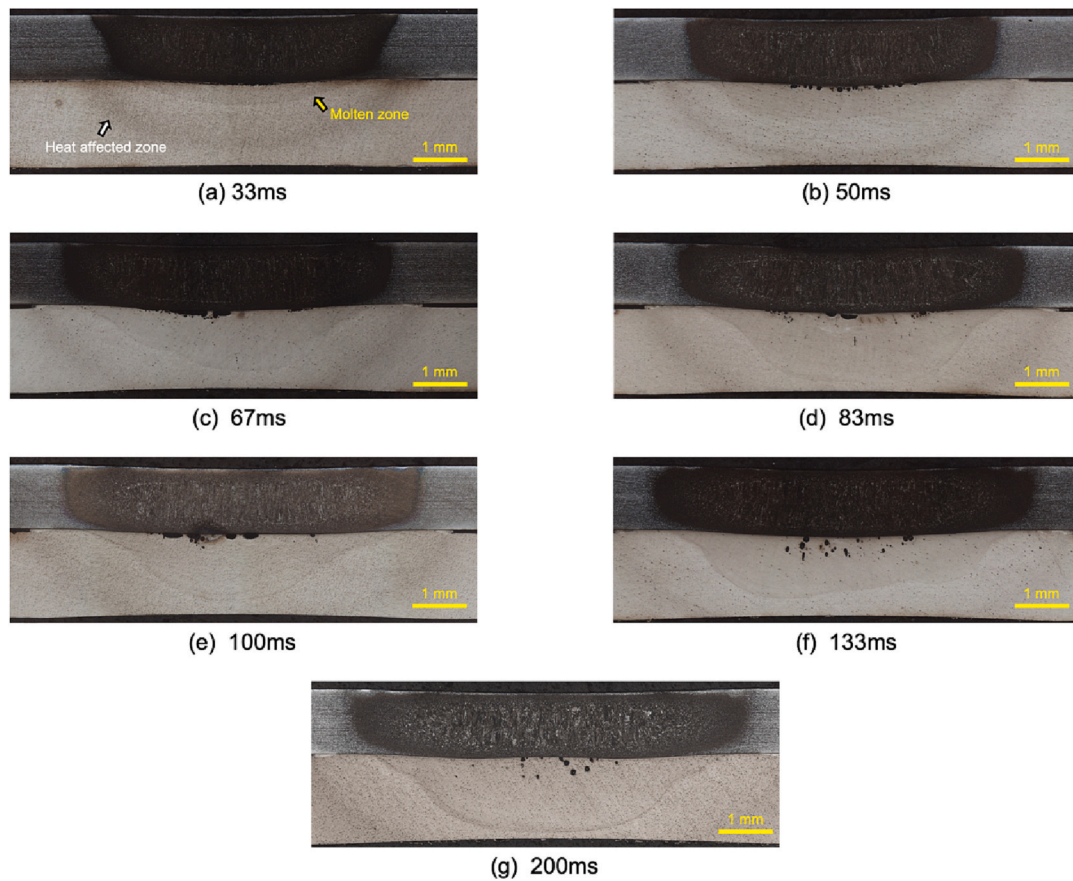


Fig. 14. Cross-sectional images for different current application times.

expected from the direct observation. Focusing on the shape of the microstructure in Fig. 15(b) to (e), it can be confirmed that there is a particular growth direction. However, the direction of growth does not coincide with the direction of convection. This is due to the fact that convection is a phenomenon during current application, and the solidification of the molten zone is a phenomenon after the end of current application. In other words, the shape of the microstructure in the molten zone depends on the temperature gradient during cooling, regardless of the effect of convection. On the other hand, focusing on the size of the microstructure, the microstructure in Fig. 15(d) appears to be larger than the other observed areas. These results suggest that it is possible that there is a correspondence between the magnitude of the convection velocity and the temperature distribution in the molten zone.

4.2. Overview of convection and convection speed

The mechanism of convection in molten aluminum alloy is discussed. Tsukiji et al. [28] examined convection in aluminum alloy during RSW of steel and aluminum alloy by numerical simulations using the smoothed-particle hydrodynamics method. The simulation results for convection obtained in the present study indicate that it occurs in the same direction as observed experimentally. Also, the electromagnetic force generated during RSW is the dominant cause of such convection. During RSW, the electromagnetic force acts in the direction toward the weld center, for both the interface and electrode sides. In other words, in the aluminum alloy molten zone, the electromagnetic force always acts in the radial direction and always inward. However, although the direction of the electromagnetic force is always the same for both the interface and electrode sides, its magnitude differs, being stronger on the electrode side. Therefore, as shown in Fig. 16, in the aluminum alloy molten zone, three types of convection occur: convection from the

center of the molten zone to the edge in the radial direction, convection from the edge of the molten zone along the bottom to the center of the molten zone, and convection from the center of the bottom of the molten zone to the interface. Thus, the experimentally observed convection, as in the simulation, is assumed to be caused by the electromagnetic force generated during welding.

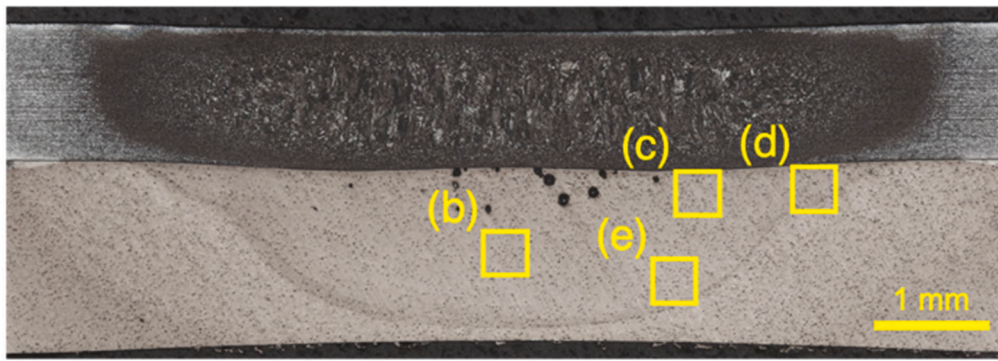
4.3. Convection focused at edge of molten zone

In this section, the effects of convection at the edge of the molten zone are considered. The experimental results suggest that convection is extremely small at the edge of the molten zone because tracer particles become accumulated in this region. As seen in Fig. 17, there is a region of shallow melt penetration at the edge of the molten zone. These results suggest that convection at the edge of the molten zone affects the shape of the molten zone. This is consistent with the results of the numerical simulations, which indicate no reduction in convection at the edge of the molten zone, and that the molten zone is bowl-shaped with no shallow melt-in region.

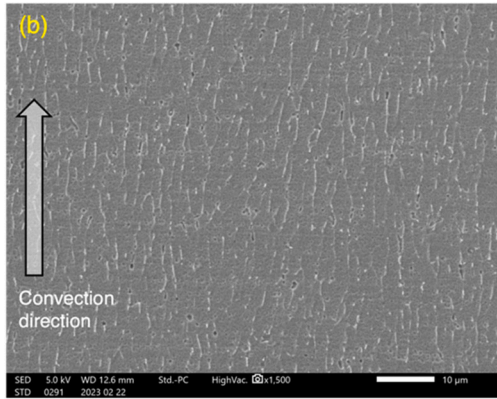
5. Conclusions

In this study, direct observation of convection was attempted using synchrotron radiation at SPring-8 for a molten aluminum alloy during RSW of steel and aluminum alloy. The results obtained are as follows.

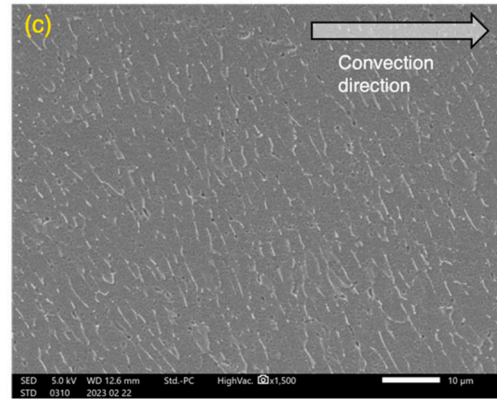
- The tracer particles installed in the aluminum alloy were observed to move as the current applied through the aluminum alloy. This is thought to be due to the movement of the tracer particles in the convection current of the molten aluminum alloy.



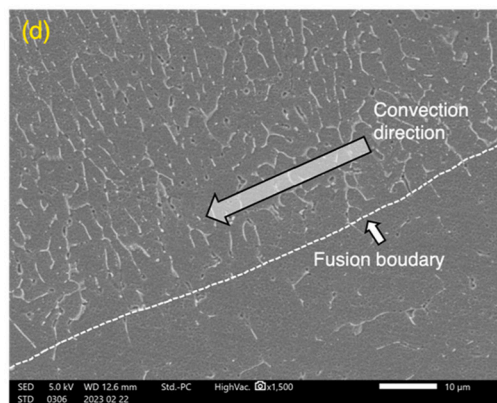
(a) Location of microstructure observation



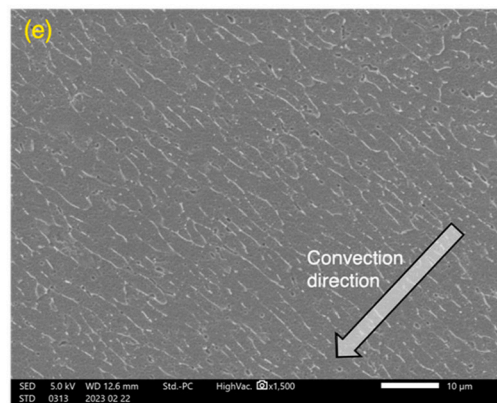
(b) Microstructure of (b) location



(c) Microstructure of (c) location



(d) Microstructure of (d) location



(e) Microstructure of (e) location

Fig. 15. SEM images for each molten zone.

- Three types of convection were observed: radial outward convection from the center of the molten zone at the joining interface, convection from the edge of the molten zone toward its center, and weak circulating convection at the edge of the molten zone.
- Extremely small convection velocities were generated at the edge of the molten zone.
- The convection velocity inside the molten zone was calculated to be approximately 1.75 m/s.
- The relationship between the shape and microstructure of the molten zone and convection was examined, and it was shown that there is a relationship between the macroscopic shape of the molten zone and convection behavior.

- The macroscopic convection behavior observed in this experiment is in good agreement with the simulation results of previous study. On the other hand, convection with a small driving force at the edge of the molten zone, which was not calculated in the simulation, was observed only in this experiment.

Declaration of competing interest

The authors declare that they have no known competing financial interests or personal relationships that could have appeared to influence the work reported in this paper.

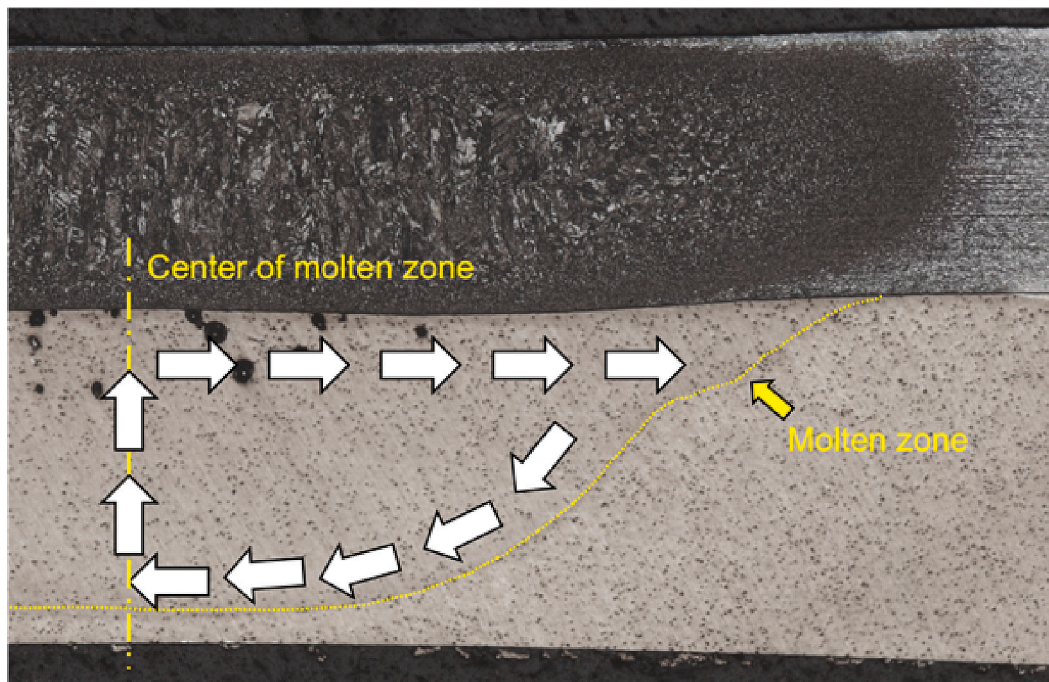


Fig. 16. Direction of convection in molten zone.

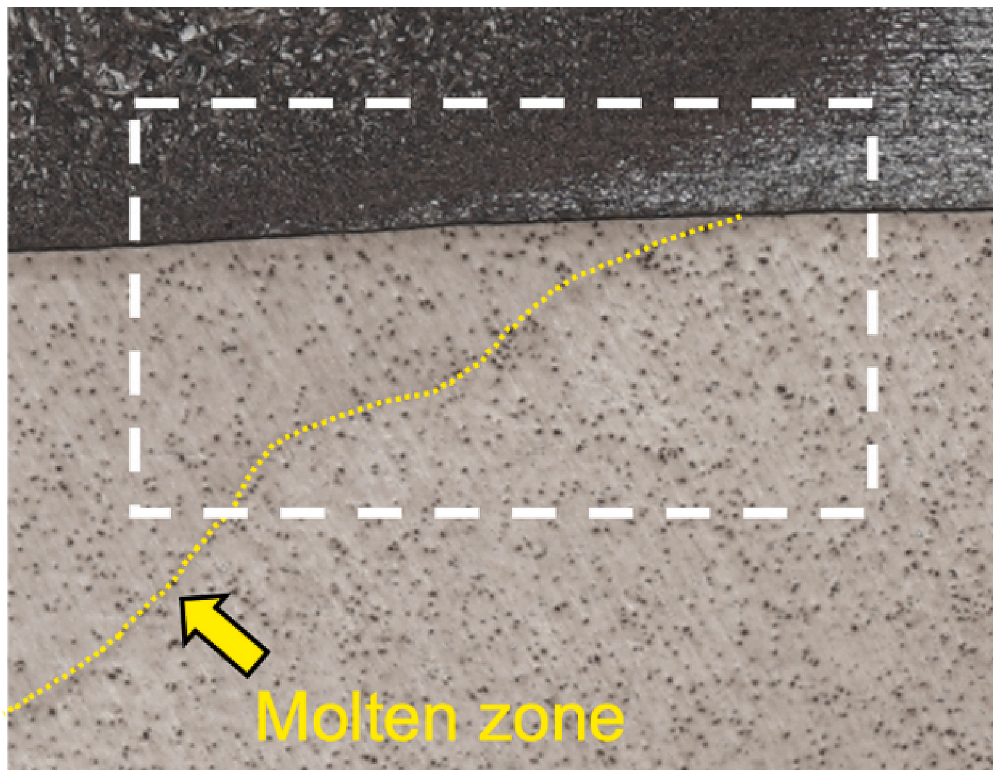


Fig. 17. Shape at edge of molten zone.

Acknowledgements

This paper is based on results obtained from a project, JPNP14014, commissioned by the New Energy and Industrial Technology Development Organization (NEDO). The synchrotron radiation experiments were performed at the BL14B1 of SPring-8 with the approval of the Japan Synchrotron Radiation Research Institute (JASRI) (Proposal No.

2020A3689 and 2019B3689). The authors would like to thank Dr. Shiro of QST for her significant help with the fundamental experiments at BL14B1 and technical support for this experiment. Also, we would like to thank Mr. Kawakami, Mr. Akizuki, Ms. Takei, Mr. Nagase, Mr. Tachibana, Mr. Koizumi, Mr. Funabiki and Mr. Ogishi, students of Osaka Institute of Technology, for conducting many experiments related to this research.

Appendix A. Supplementary data

Supplementary data to this article can be found online at <https://doi.org/10.1016/j.jmapro.2023.03.032>.

References

- [1] Miyamoto K, Nakagawa S, Sugi C, Sakurai H, Hirose A. Dissimilar joining of aluminum alloy and steel by resistance spot welding. *SAE Int J Mater Manuf* 2009; 2(1):58–67.
- [2] Zhang W, Sun D, Han L, Liu D. Interfacial microstructure and mechanical property of resistance spot welded joint of high strength steel and aluminium alloy with 4047 AlSi12 interlayer. *Mater Des* 2014;57:186–94.
- [3] Arghavani MR, Movahedi M, Kokabi AH. Role of zinc layer in resistance spot welding of aluminum to steel. *Mater Des* 2016;102:106–14.
- [4] Wan Z, Wang HP, Chen N, Wang M, Carlson BE. Characterization of intermetallic compound at the interfaces of Al-steel resistance spot welds. *J Mater Process Technol* 2017;242:12–23.
- [5] Chen N, Wan M, Wang HP, Wan Z, Carlson BE. Microstructure and mechanical evolution of Al/steel interface with Fe2Al5 growth in resistance spot welding of aluminum to steel. *J Manuf Process* 2018;34:424–34.
- [6] Pan B, Shang SL, Banu M, Wang PC, Carlson BE, Liu ZK, Li J. Understanding formation mechanisms of intermetallic compounds in dissimilar Al/steel joint processed by resistance spot welding. *J Manuf Process* 2022;83:212–22.
- [7] Zhang W, Sun D, Han L, Li Y. Optimized design of electrode morphology for novel dissimilar resistance spot welding of aluminium alloy and galvanized high strength steel. *Mater Des* 2015;85:461–70.
- [8] Sun D, Zhang Y, Liu Y, Gu X, Li H. Microstructures and mechanical properties of resistance spot welded of 16Mn steel and 6063–T6 aluminum alloy with different electrodes. *Mater Des* 2016;109:596–608.
- [9] Shi L, Kang J, Amirkhiz BS, Sigler DR, Haselshuhn AS, Carlson BE. Influence of sheet thickness ratio on fracture mechanisms of Al-steel resistance spot welds produced using multi-ring domed electrode. *Sci Technol Weld Join* 2020;25(2): 164–8.
- [10] Hu S, Haselshuhn AS, Ma Y, Li Y, Carlson BE, Lin Z. Influencing mechanism of inherent aluminum oxide film on coach peel performance of baked Al-steel RSW. *Mater Des* 2021;197:109250.
- [11] Shi L, Kang J, Qian C, Liang J, Amirkhiz BS, Haselshuhn AS, Carlson BE. Role of Fe2Al5 in fracture of novel dissimilar aluminum-steel resistance spot welds using multi-ring domed electrodes. *Mater Sci Eng A* 2022;831:142233.
- [12] Das T, Das R, Paul J. Resistance spot welding of dissimilar AISI-1008 steel / Al-1100 alloy lap joints with a graphene interlayer. *J Manuf Process* 2020;53:260–74.
- [13] Lara B, Giorjao R, Ramirez A. Resistance spot welding of printed interlayers to join Al-Fe sheets. *Sci Technol Weld Join* 2023;28(1):18–26.
- [14] Hu S, Haselshuhn AS, Ma Y, Li Z, Qi L, Li Y, Carlson BE, Li Z. Effect of external magnetic field on resistance spot welding of aluminium to steel. *Sci Technol Weld Join* 2022;27(2):84–91.
- [15] Li P, Chen S, Dong H, Ji H, Li Y, Guo X, Yang G, Zhang X, Han X. Interfacial microstructure and mechanical properties of dissimilar aluminum/steel joint fabricated via refilled friction stir spot welding. *J Manuf Process* 2020;49:385–96.
- [16] Cui L, Wei Z, Ma B, He D, Huang H, Cao Q. Microstructure inhomogeneity of dissimilar steel/Al butt joints produced by laser offset welding. *J Manuf Process* 2020;50:561–72.
- [17] Abe Y, Fujimoto T, Nakatani M, Komen H, Shigeta M, Tanaka M. High speed X-ray observation of digital controlled submerged arc welding phenomena. *Sci Technol Weld Join* 2021;26(4):332–40.
- [18] Yamazaki K, Asano R, Toda R, Saito Y, Shigeta M, Tanaka M. Observation of phenomena in the slag Bath during electroslag welding. *Q J Jpn Weld Soc* 2021;39(4):347–62 [in Japanese].
- [19] Komen H, Abe Y, Fujimoto T, Shigeta M, Nakatani M, Tanaka M. Visualization of submerged arc welding phenomena by X-ray observation and direct observation. *Weld Lett* 2018;36(4):9–12.
- [20] Miyagi M, Wang H, Yoshida R, Kawahito Y, Kawakami H, Shobu T. Effect of alloy element on weld Pool dynamics in laser welding of aluminum alloys. *Sci Rep* 2018; 8:12944.
- [21] Komen H, Shigeta M, Tanaka M, Abe Y, Fujimoto T, Nakatani M, Anthony Murphy B. Numerical investigation of heat transfer during submerged arc welding phenomena by coupled DEM-SPH simulation. *Int J Heat Mass Transf* 2021;17: 121062.
- [22] Komen H, Shigeta M, Tanaka M, Nakatani M, Abe Y. Numerical simulation of slag forming process during submerged arc welding using DEM-SPH hybrid method. *Weld World* 2018;62(6):1323–30.
- [23] Komen H, Shigeta M, Tanaka M. Numerical simulation of molten metal droplet transfer and weld pool convection during gas metal arc welding using incompressible smoothed particle hydrodynamics method. *Int J Heat Mass Transf* 2018;121:978–85.
- [24] Komen H, Shigeta M, Tanaka M, Fukunishi Y. Incompressible SPH simulation of weld Pool convection with molten metal droplets in a GMA welding. *Q J Jpn Weld Soc* 2015;33(4):332–40 [in Japanese].
- [25] Ito M, Nishio Y, Izawa S, Fukunishi Y, Shigeta M. Numerical simulation of joining process in a TIG welding system using incompressible SPH method. *Q J Jpn Weld Soc* 2015;33(2):32–8.
- [26] Ito M, Izawa S, Fukunishi Y, Shigeta M. Numerical simulation of a weld pool formation in a TIG welding using an incompressible SPH method. *Q J Jpn Weld Soc* 2014;32(4):213–22 [in Japanese].
- [27] Qi L, Zhang Q, Niu S, Chen R, Li Y. Influencing mechanism of an external magnetic field on fluid flow, heat transfer and microstructure in aluminum resistance spot welding. *Eng Appl Comput Fluid Mech* 2021;15(1):985–1001.
- [28] Chikuchi S, Shigeta M, Komen H, Tanaka M. Particle simulation of nugget formation process during steel/aluminum alloy dissimilar resistance spot welding and thickness estimation of intermetallic compounds. *Welding International*. 2022; 36(7):434–42.